OPTOELECTRONICS AND ADVANCED MATERIALS – RAPID COMMUNICATIONS Vol. 11, No. 9-10, September-October 2017, p. 555 - 559

Influence of carrier escape mechanism on the operating wavelength of InGaN/GaN multiple quantum well solar cells

SHITAO LIU[a], FEIFEI WU[a], QI YANG[a], YUANDAN HE[a], JIANLI ZHANG[b], ZHIJUE QUAN[b], HAIBIN HUANG[c], LI WANG[*]
[a]*School of Materials Science and Engineering, Nanchang University, Nanchang 330031, People's Republic of China*
[b]*National Engineering Technology Research Center for LED on Si Substrate, Nanchang University, Nanchang 330047, People's Republic of China*
[c]*Institute of Photovoltaics, Nanchang University, Nanchang 330031, People's Republic of China*

We fabricated a series of InGaN/GaN multiple quantum well solar cells with indium content varying from 0.16 to 0.32. The emission wavelengths of the samples vary from 450 nm to 570 nm at forward current density of 35A/cm^2. External quantum efficiency measurements indicate that the maximum operating wavelength of the series of solar cells ends when the emission wavelengths approache 500 nm, though some of the samples have much longer absorption edges. To explain this phenomenon, we theoretically analyzed the escape efficiency of photo-generated carriers in the multiple quantum wells (MQW). It was revealed that the carrier escape mechanism is the determining factor of maximum operating wavelength for high indium content InGaN/GaN MQW solar cells.

(Received November 3, 2016; accepted October 10, 2017)

Keyword: InGaN/GaN multiple quantum well, Solar cell, Carrier escape mechanism

1. Introduction

InGaN alloy is a promising photovoltaic (PV) material due to its tunable band gap (0.65～3.4eV), high absorption coefficient (～10^5 cm^{-1}), high carrier mobility, high saturation velocity and high radiation resistance [1,2]. Because the band gap of InGaN alloy covers almost the entire solar spectrum, it has the potential in developing high-efficiency full-spectrum response solar cells based solely on nitride-based materials [3]. Energy conversion efficiencies above 60% achieved by InGaN-based solar cells have been predicted by theoretical studies [4].

Since the first demonstration of PV response for InGaN materials in 2007 [3], considerable efforts have been poured into the study of InGaN solar cells [2, 5]. Due to the lack of lattice-matched substrate, most of the reported InGaN solar cells are fabricated on GaN templates. Because the lattice mismatch between InGaN and GaN increases with the increase of In content, growth of high quality InGaN absorption layer is generally limited within an In content of 0.12 for a comparatively thick single layer [2]. With the newly developed growth technique, Fischer *et al* demonstrated that as the In content exceeds 0.6, InGaN films exhibit a significant improvement in the crystalline quality and optical properties due to uniform full lattice-mismatch strain relaxation [6]. However, with In content set between 0.2 ~ 0.6, the growth of high quality thick InGaN film is still very difficult which makes the realization of high efficiency homo-junction InGaN solar cells with long operating wavelength to be highly challenging. For this reason, multiple quantum well (MQW) structure has been widely adopted for InGaN solar cells since it can contain more In while maintaining a crystalline quality [7-10]. That is beneficial for expanding the operating wavelength of InGaN solar cells. Even so, reports on InGaN/GaN MQW solar cell with long operating wavelength are rare [2, 11]. Lai [8] and Dahal [7,12] had reported InGaN/GaN MQW with indium content exceeds 0.3, but the maximum operating wavelength of their samples were still limited at around 500 nm. In this paper, we fabricated a series of InGaN/GaN multiple quantum well solar cells with different indium content and studied the dependence of operating wavelength on carrier escape mechanism. Our results show that the maximum operating wavelength is limited by the carrier escape mechanism for InGaN/GaN MQW solar cells with high indium content.

2. Experimental methods

We prepared a series of samples with indium content varying from 0.16 to 0.32 by metal organic vapor deposition (MOCVD) on GaN/Si templates. The layer structures of the samples are illustrated in Fig. 1. The MQWs with different target In content were grown under the established growth conditions of high efficiency LED [13]. After epi-layer growth, an Ag layer of 100 nm thickness was deposited on the p-GaN layer. It acts as the p-type contact as well as the light reflector. Then the

epi-wafers were bonded to the supporting Si substrates and the growth substrates were removed by chemical etching. The exposed n-type layer was roughened by KOH solution and then an Al/Ti/Au n-type contact was prepared on the roughened surface. It was in that process that, p-side down vertical-structured InGaN/GaN MQW solar cells with 1mm × 1mm chip size were fabricated. A p-side up sample with similar InGaN/GaN MQW structure was prepared on sapphire substrate for comparison. The emission wavelengths of the samples were measured by applying a forward current of 350 mA to verify the band gap (and In content) of the samples. The external quantum efficiency and absorption spectra were measured as a function of wavelength to study the carrier generation and escape in the samples. The absorption spectra were measured by collecting the reflected light with an integrating sphere placed over the device. Because there was an Ag reflector deposited on the p-GaN layer in these samples, the absorption can be obtained by subtracting the reflected light from the incident light.

p-GaN layer, 130nm
7 MQWs InGaN/GaN(2.5/10nm), x=0.16~0.32
InGaN/GaN super lattice, x=0.04
n-GaN layer, 2μm
Substrate

Fig. 1. (black and white) Layer structure of samples

3. Results and discussion

Fig. 2(a) shows the samples of the normalized electroluminescence (EL) spectra. The EL peak positions of the eight samples are 450 nm, 480 nm, 510 nm, 521 nm, 527 nm, 531 nm, 550 nm and 570 nm, respectively. We label the samples as sample A, B, C, D, E, F, G and H, respectively. Sample G (550 nm) is grown on sapphire substrate and all the others are grown on Si substrate. The EL spectra indicate that we have obtained high quality InGaN/GaN MQW solar cells with considerably high indium content. From the light absorption point of view, operating wavelength far above 500 nm can be expected in sample D, E, F, G and H. Fig. 2(b) shows the external quantum efficiency (EQE) as a function of wavelength. From the peak 380nm to shorter wavelengths, the EQEs abruptly drop to 0 within a few nanometers. This efficiency loss is due to the surface absorption of the thick n-GaN layer. The EQE curve shape of sample G is slightly different to others due to its p-side up structure. In addition, The EQE of all the samples decrease as the wavelengths grow, to which the quantum that confined stark effect (QCSE) in the quantum wells are attributed [14]. For sample A and B, their EQE curves end at about 445 nm and 475 nm, respectively, which are in accordance with their emission peak positions. However, it is striking that the EQE curves of all the other samples end at about 500 nm, though some of them have much longer emission wavelengths. For further understanding, we measured the absorption spectra of sample D and H to confirm their absorption edge. The absorption spectra are presented in Fig. 3. We can see that the absorption spectra of sample D and H extend to 520 nm and 570 nm, respectively, which are in consistent with their emission wavelengths. That result indicates that the absorption of light with wavelength longer than 500 nm does not generate photocurrent in these samples.

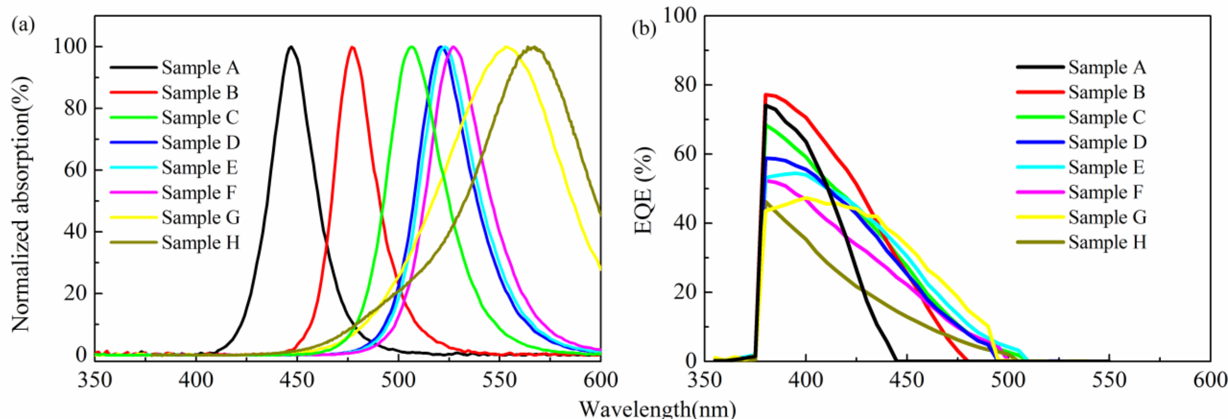

Fig. 2. (Color online)(a) EL spectra of samples.(b) EQE spectra of InGaN/GaN MQW solar cells with different wavelength

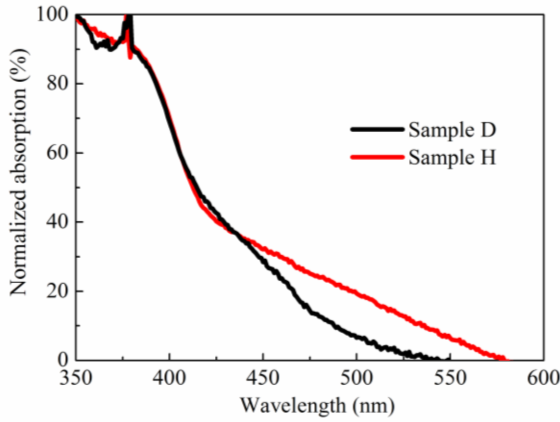

Fig. 3. (Color online) Absorption of InGaN/GaN MQW solar cells with different wavelength

To understand the missing photocurrent for wavelengths longer than 500 nm, it is necessary for us to analyze all of the processes of the photo-generated carriers in a MQW solar cell. In consideration of an electron's situation, we conclude it can: (i) absorb incident photon energy then transfer itself from the valence band to the conduction band, (ii) escape from the quantum well by tunneling or thermionic emission, (iii) recombine with a hole. In most cases, process (i) depends on the absorption of the solar cell, and the escape efficiency depends on the competition between process (ii) and (iii). Fig. 4 gives the schematic diagram of the carrier transport mechanism in a quantum well. To simplify the discussion, we assume that all the carriers escaped from the quantum wells can be collected by the electrodes and ignore other losses. So the collection efficiency $\eta_{collection}$ of solar cells can be described as:

$$\eta_{collection} = \frac{\dfrac{1}{\tau_T} + \dfrac{1}{\tau_{TE}}}{\dfrac{1}{\tau_T} + \dfrac{1}{\tau_{TE}} + \dfrac{1}{\tau_R}} \quad (1)$$

In equation (1), τ_R is the recombination life time, τ_{TE} is the thermionic emission life time and τ_T is the tunneling life time of electron. According to the Wentzel-Kramers-Bruillouin (WKB) approximations, the electron tunneling lifetime can be calculated by [14, 15]:

$$\frac{1}{\tau_T} = \frac{\pi}{2L_w^{\ 2} m^*} \exp \int_0^{L_b} -2\sqrt{\frac{2m^*(E_c(x) - E)}{2}}\, dx \quad (2)$$

The thermionic emission lifetime can be calculated by [15]:

$$\frac{1}{\tau_{TE}} = \left(\frac{k_B T}{2\pi m^* L_w}\right)^{1/2} \exp\left(-\frac{E_{c\max} - E}{k_B T}\right) \quad (3)$$

In equations (2) and (3), L_w and L_b are quantum well and quantum barrier thickness, respectively. The effective mass of electron m^* used here is $0.169m_0$ [14]. E is the electron energy after absorbing the incident photon energy, $E_c(x)$ and E_{cmax} are the conduction band energy at position x and the maximum conduction band energy in the barrier, respectively. k_B is Boltzmann's constant and T is the absolute temperature.

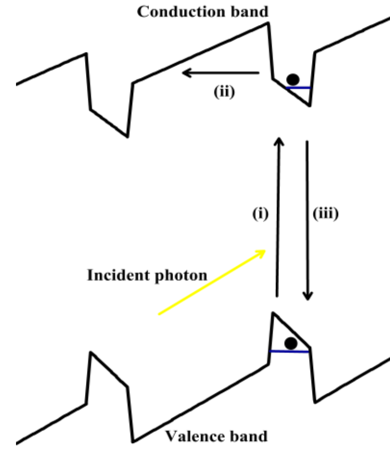

Fig. 4. (Color online) Schematic illustration of the processes of the photo-generated carriers. (i) absorbs incident photon energy and gets to the conduction band from the valence band, (ii) escapes from the quantum well by tunneling or thermionic emission, (iii) recombines with a hole. Black dot means electron, and blue line means energy state

To obtain the energy levels for carrier escape probability calculation, we utilized the Silvaco ATLAS program [16] to simulate the band structure of the MQWs. The ATLAS program can self-consistently solve Poisson's equation and the carrier drift–diffusion equation. In the simulations, the physical models of the polarization effect and Shockley–Read–Hall (SRH) recombination are included. The primary material parameters of GaN and InN used in the simulations are listed in Table 1 [17]. For InGaN alloy, the parameters were calculated using the Vegard's Law. The band gap was determined by the emission wavelength. By simulations we obtained $E_c(x)$ and E_{cmax} of the samples. To calculate the escape lifetime of an electron through equations (2) and (3), the energy level E should be known. In bulk materials, the photo-generated carriers usually thermalize (relax to the bottom of conduction band and valence band) in a very short time (~ps). In previous study of InGaN/GaN MQW solar cells, similar fast thermalization was assumed and the ground state energy (n=1) was used to calculate the escape probability [14]. Based on the same assumption, the tunneling and thermionic emission lifetime for sample D and H were calculated. For sample D, the tunneling lifetime and thermionic emission lifetime are 378.6 ns and 1.56μs, respectively. For sample H, the tunneling lifetime and thermionic emission lifetime are 4.29 μs and 679 μs,

respectively. The calculated lifetimes are quite long, mainly due to the high energy barriers caused by the high indium content in the quantum wells. Because the reported carrier recombination lifetime in InGaN/GaN MQW are typically less than 100 ns [18,19], the carrier collection efficiency calculated using equation (1) should be nearly 0. Furthermore, because of the fast thermalization, the carrier escape lifetime should be independent to the excitation light wavelength. That is clearly opposite to our experimental results. The EQE curve given in Fig. 2(b) shows that both sample D and sample H have considerable efficiency in the short wavelength range. As has been pointed out by Lang, escape from the ground state denotes the "worst-case" because in this case the energy barrier for carrier escape is the highest. For InN, hot-carriers have been predicted theoretically to have a long lifetime due to its beneficial phonon structure, known as the phonon bottleneck effect [1]. And a relatively long hot-carrier lifetime of ~20ps has been experimentally observed in InN by Chen *et al* [20]. Moreover, in InGaN/GaN MQW, due to the small size of the quantum well and the high confining potentials, it is difficult for the generated carriers to reach equilibrium distribution and have great chance to escape the quantum well from high energy levels [21,22]. Based on these facts, the carrier thermalization process is ignored, and we assume all the carriers escape from the exited state. This is the "best-case" for carrier escape. In that case, we assume a carrier recombination lifetime of 1 ns [23], we can obtain the carrier collection efficiency by equation (1), (2) and (3). It can be seen from Fig. 5 that when the wavelength is lower than 410nm, the collection efficiency is 1. Because the potential barrier of carriers excited by high photo energy is low, the carriers can escape easily. For longer wavelength, the collection efficiency drops quickly to 0. The collection efficiency is sensitive to photo energy because the tunneling and thermionic emission lifetime is exponentially dependent on the energy level the electron occupied. From Fig. 5(b), we can conclude that the operating wavelength increases as the indium content in low indium content range grows, the maximum operating wavelength doesn't increase and ends at about 500nm, which is consistent with our experiment results. It should be pointed out that for a real InGaN/GaN MQW solar cell, the carrier escape probability should be lower than the "best-case", so the above calculated maximum operating wavelength should be the upper limit. On the other hand, if the carrier recombination lifetime is longer than 1 ns, the operating wavelength should be longer.

Table 1. Parameters of GaN and InN used for simulation

Parameter	GaN	InN
Lattice constant(Å)	3.548	3.189
Band gap Eg(eV)	3.42	0.65
Dielectric constant $\varepsilon_s/\varepsilon_0$	8.9	10.5
Electron mass m_e/m_0	0.2	0.05
Hole mass m_e/m_0	1.25	0.6
μ_e ($cm^2V^{-1}s^{-1}$)	350	350
μ_h ($cm^2V^{-1}s^{-1}$)	3	3

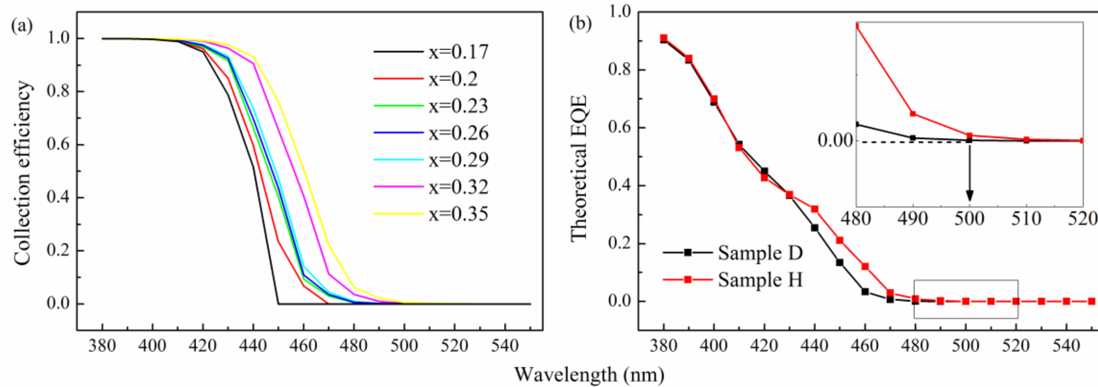

Fig. 5. (Color online) (a) The collection efficiency with different indium content as a function of wavelength. (b) The theoretical efficiency of Sample D and H with different wavelength. Black arrow points to the operating wavelength (~500 nm), the inset is enlarge view

Using the data shown in Fig. 3, we can calculate the EQE with different wavelength by:

$$EQE(\lambda) \propto \eta_{collection}(\lambda) \times G(\lambda) = \eta_{collection}(\lambda) \times \alpha(\lambda) \quad (4)$$

In equation (4), G is carrier generation rate, here we set it to be equal to the absorption rate. So we can get the theoretical EQE as a function of wavelength, as shown in Fig. 5 (b). The results of theoretical EQE notoriously coincide with experimental results which provide a strong evidence to show that the escape mechanism is a decisive factor to operating wavelength when indium content is high.

4. Conclusions

In summary, we fabricated high indium content InGaN/GaN MQW solar cell with absorption edge extending to 560 nm. But external quantum efficiency measurements showed that the operating wavelength of the solar cell is much shorter than the absorption edge, which reveals the operating wavelength dependence on carrier escape mechanism. Our results verified showed the vital demands of optimization of device structure to improve carrier transport for InGaN/GaN MQW solar cells.

Acknowledgments

The authors acknowledge the support from National Natural Science Foundation of China (Grant No. 61564007) and Jiangxi provincial Sci-Tech Support Plan (Grant No. 20141BBE50035).

References

[1] J. Wu, J. Appl. Phys. **106**(1), 011101 (2009).
[2] A. G Bhuiyan, K. Sugita, A. Hashimoto, A. Yamamoto, IEEE J. Photovolt. **2**(3), 276 (2012).
[3] O. Jani, I. Ferguson, C. Honsberg, S. Kurtz, Appl. Phys. Lett. **91**(13), 132117 (2007).
[4] A. Luque, A. Marti, Phys. Rev. Lett. **78**(26), 5014 (1997).
[5] D. Mclaughlin, J. Pearce, Metall. Mater. Trans. A, **44A**(4), 1947 (2013).
[6] A. M. Fisher, Y. O. Wei, F. A. Ponce, M. Moseley, B. Gunning, W. A. Doolittle, Appl. Phys. Lett. **103**(13), 131101 (2013).
[7] R. Dahal, B. Pantha, J. Li, J. Y. Lin, H. X. Jiang, Appl. Phys. Lett. **94**(6), 063505 (2009).
[8] K. Y. Lai, G J. Lin, Y. L. Lai, Y. F. Chen, J. H. He, Appl. Phys. Lett. **96**(8), 081103 (2010).
[9] S. Valdueza-Felip, A. Mukhtarova, L. Grenet, C. Bougerol, C. Durand, J. Eymery, E. Monroy, Appl. Phys. Express **7**(3), 032301 (2014).
[10] S. Choi, J. Shim, D. Kim, H. Jeong, Y. Jho, Y. Song, D. Lee, Appl. Phys. Lett. **103**(3), 033901 (2013).
[11] L. Redaelli, A. Mukhtarova, S. Valdueza-Felip, A. Ajay, C. Bougerol, C. Himwas, J. Faure-Vincent, C. Durand, J. Eymery, E. Monroy, Appl. Phys. Lett. **105**(13), 131105 (2014).
[12] R. Dahal, J. Li, K. Aryal, J. Y. Lin, H. X. Jiang, Appl. Phys. Lett. **97**(7), 073115 (2010).
[13] J. Zhang, C. Xiong, J. Liu, Z. Quan, L. Wang, F. Jiang, Appl. Phys. A **114**(4), 1049 (2014).
[14] J. R. Lang, N. G Young, R. M. Farrell, Y. R. Wu, J. S. Speck, Appl. Phys. Lett. **101**(18), 181105 (2012).
[15] M. Singh, J. Singh, J. Appl. Phys. **91**(5), 2989 (2002).
[16] ATLAS User's Manual 2012, see http://www.silvaco.com.
[17] I. Vurgaftman, J. R. Meyer, L. R. Ram-Mohan, Journal of Applied Physics **89**(11), 5815 (2001).
[18] Z. Z. Bandic, P. M. Bridger, E. C. Piquette, T. C. McGill, Appl. Phys. Lett. **72**(24), 3166 (1998).
[19] F. Chen, A. N. Cartwright, H. Lu, W. J. Schaff, Phys. Status Solidi A **202**(5), 768 (2005).
[20] F. Chen, A. N. Cartwright, H. Lu, W. J. Schaff, Appl. Phys. Lett. **83**(24), 4984 (2003).
[21] C. S. Xia, W. D. Hu, C. Wang, Z. F. Li, X. S. Chen, W. Lu, Z. M. Simon Li, Z. Q. Li, Optical and Quantum Electronics. **38**(12-14), 1077 (2006).
[22] X. Ni, X. Li, J. Lee, S. Liu, V. Avrutin, U. Ozgiir, H. Morkoc, A. Matulionis, Journal of Applied Physics **108**(3), 033112 (2010).
[23] Sang-Bae Choi, Jae-Phil Shim, Dong-Min Kim, Hoon-Il Jeong, Young-Dahl Jho, Young-Ho Song, Dong-Seon Lee, Applied Physics Letters **103**(3), 033901 (2013).

*Corresponding author: wl@ncu.edu.cn